Journal of Power Sources 196 (2011) 9552–9560

Contents lists available at ScienceDirect

Journal of Power Sources

journal homepage: www.elsevier.com/locate/jpowsour

Synthesis of mesoporous carbon-silica-polyaniline and nitrogen-containing carbon-silica films and their corrosion behavior in simulated proton exchange membrane fuel cells environment

Tao Wang, Jianping He*, Dun Sun, Yunxia Guo, Yiou Ma, Yuan Hu, Guoxian Li, Hairong Xue, Jing Tang, Xin Sun

College of Material Science and Technology, Nanjing University of Aeronautics and Astronautics, Nanjing 210016, PR China

ARTICLE INFO

Article history:
Received 6 July 2011
Received in revised form 28 July 2011
Accepted 29 July 2011
Available online 4 August 2011

Keywords:
Nitrogen-containing
Mesoporous carbon-silica
Electropolymerization
Stainless steel
Acid corrosion

ABSTRACT

In this study, polyaniline is deposited onto mesoporous carbon-silica-coated 304 stainless steel using electropolymerization method. Variation of the electropolymerization time and applied potential can affect the growth of polyaniline, and lead to different structural and electrochemical properties of the films. Nitrogen-containing groups are successfully introduced onto the mesoporous carbon-silica film by pyrolyzing treatment under N_2 atmosphere and the electrical conductivity is improved observably compared with the carbon-silica film. The electrochemical properties of the mesoporous carbon-silica-polyaniline films and nitrogen-containing carbon-silica composite films are examined by using potentiodynamic polarization, potentiostatic polarization and electrochemical impedance spectroscopy. The corrosion tests in 0.5 M H_2SO_4 system display that the carbon-silica-polyaniline films show the optimal protective performance. However, according to potentiostatic polarization process, nitrogen-containing carbon-silica film with a water contact angle 95° is extremely stable and better for the protection of stainless steel in simulated fuel cell environment compared to carbon-silica-polyaniline film. Therefore, the nitrogen-containing carbon-silica-coated 304 stainless steel is a promising candidate for bipolar plate materials in PEMFCs.

1. Introduction

Proton exchange membrane fuel cells (PEMFCs) have been widely considered to power transportation vehicles such as automobiles and buses due to their high power density, relatively quick start-up, low operating temperatures and low greenhouse gas emissions [1,2]. Bipolar plates constitute the backbone of a PEMFCs power stack, which are mainly used to distribute and separate reactant gases and to collect and transmit electric current. The requirements of materials suitable for use as bipolar plates are high electric conductivity, high corrosion resistance, high mechanical strength, high gas impermeability, light material, and low-cost material. In recent years, more and more studies showed that stainless steels such as 304, 310, 316 and 321 stainless steels, may be promising bipolar plate materials to satisfy commercial applications of PEMFCs [3,4]. However, stainless steels as bipolar plates develop a passivating oxide layer on the surface that does protect the bulk metal from progression of corrosion, but also cause an undesirable effect of a high surface contact resistance, which is a severe problem since it affects the lifetime and performance of a PEMFC. Coatings using metal-based or carbon-based materials which should be conductive and adhere to the base metal without exposing the substrate to corrosive media, have been investigated to protect stainless steel bipolar plates by providing high corrosion resistance and low contact resistance [5–10]. Carbon-based coatings with low surface energy, low water contact angle (≥90° and high) surface wetability on bipolar plates could directly contribute to flooding of cathode side of the fuel cell. So far, various carbonaceous materials, such as graphite, conductive polymer, diamond-like carbon, and organic self-assembled monopolymers, have been used as carbon-based coatings to bipolar plates [10–14].

Chen et al. [9] tried to improve the performance of 304 stainless steel bipolar plates by coating a nickel layer to catalyze carbon deposits at 680 °C under C_2H_2/H_2 mixed gas atmosphere, and a continuous carbon film with compact structure was obtained. The carbon film composed of a highly ordered graphite layer and a surface layer with disarranged graphite structure revealed excellent chemical stability similar to high-purity graphite plate. It is well known that passive film on stainless steel protects the bulk of it from corrosion, but causes a decrease in the interfacial contact resistance between the bipolar plate and gas diffusion layer because passive film is usually composed of mixed metal oxides.

* Corresponding author. Tel.: +86 25 52112626; fax: +86 25 52112626.
E-mail address: jianph@nuaa.edu.cn (J. He).

0378-7753/$ – see front matter © 2011 Elsevier B.V. All rights reserved.
doi:10.1016/j.jpowsour.2011.07.084

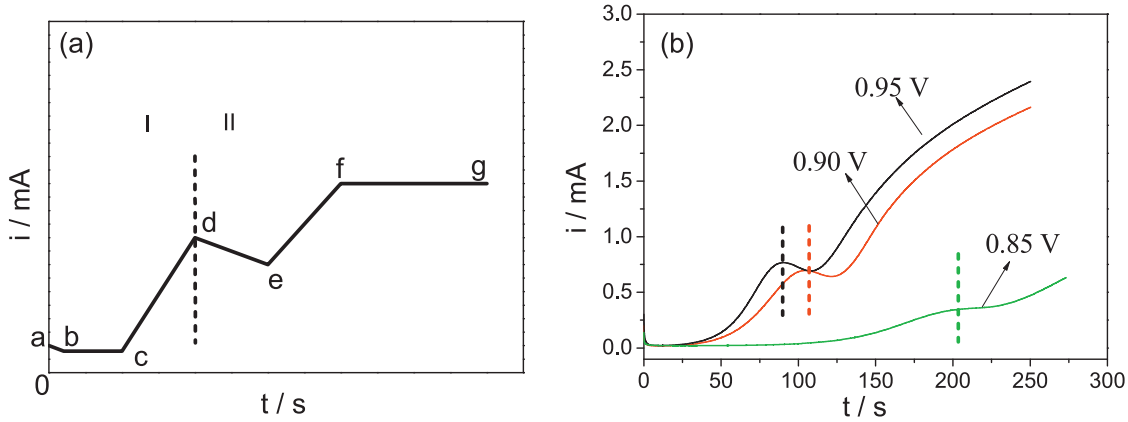

Fig. 1. Simulative current–time transient (a) and actual current–time transients (b), traced during the PANI electropolymerization on mesoporous C-SiO_2 film from 0.5 M H_2SO_4 containing 0.2 M aniline at different constant potentials: 0.85 V, 0.90 V and 0.95 V.

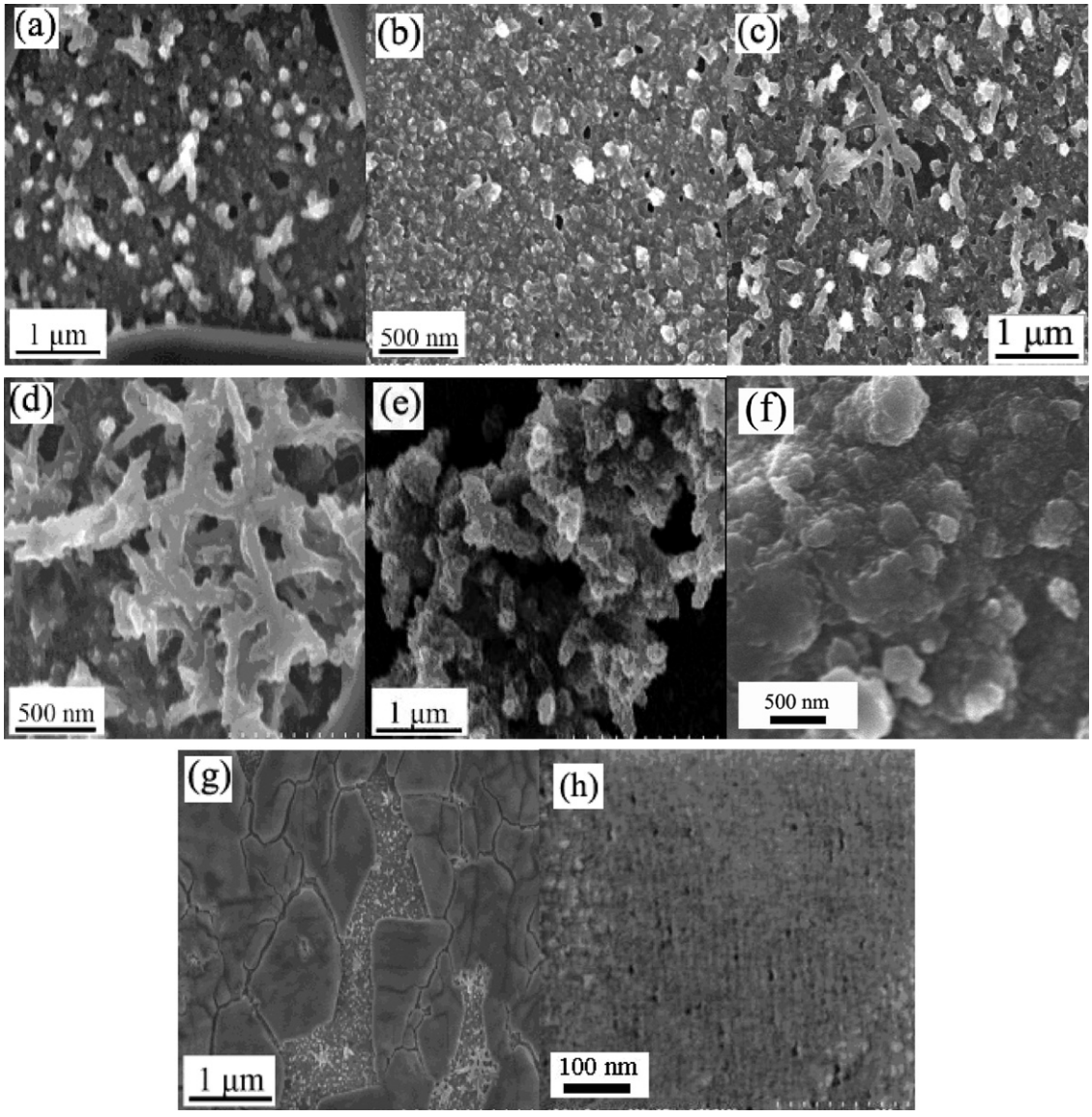

Fig. 2. SEM images of the PANI-C-SiO_2 films synthesized under potentiostatic conditions upon varying the electropolymerization time: (a) and (b) 200, (c) and (d) 250, (e) and (f) 300, (g) 400 s, at 0.85 V (SCE), and the C-SiO_2 film (h).

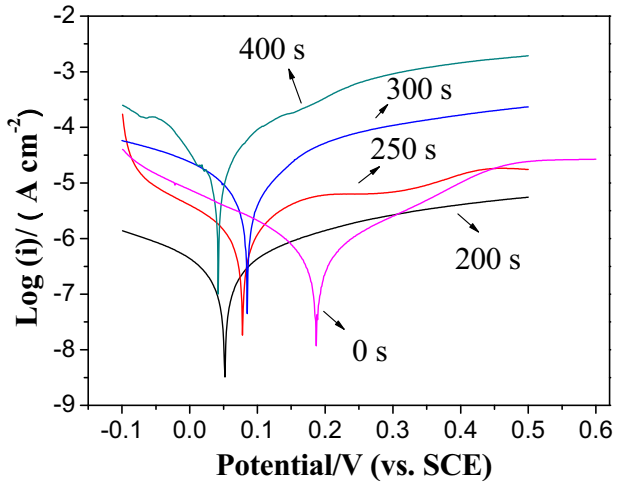

Fig. 3. Potentiodynamic polarization curves of the PANI-C-SiO_2 films synthesized under potentiostatic conditions upon varying the electropolymerization time: 200, 250, 300, 400 s, at 0.85 V (SCE), and the C-SiO_2 film (0 s) in 0.5 mol L^{-1} H_2SO_4 solution.

In order to impart low interfacial contact resistance to stainless steel, Fukutsuka et al. [10] applied plasma-assisted chemical vapor deposition coating of carbon film on the 304 stainless steel and compared the performance with the 304 stainless steel. The corrosion protection was better determined by dynamic polarization curves in spite of the absence of passive film. They thought that corrosion resistance of carbon-coated 304 stainless steel depended on the polishing process of the 304 stainless steel, but the reason was not clarified. Compared to other coating materials, a conductive polymer coating can be formed easily on metal surfaces using electropolymerization methods [7,15–18]. Joseph et al. [17] investigated the corrosion behavior of the 304 stainless steel coated with the conducting polymers polyaniline (PANI) and polypyrrole. The polymer-coated stainless steel plates showed improved corrosion resistance with acceptable contact resistance, but their cost, durability, and volume production were not mentioned in the study. González and Saidman [18] observed an efficient corrosion protection by studying the electrosynthesis of polypyrrole films onto 316L stainless steel.

A new approach is coating a mesoporous film on stainless steel substrate by spin-coating method, which may integrate the advantages of porous materials into metallic bipolar plate. According to the literature data [12], the major forms of carbon-silica deposits are mesoporous rather than a compact film. Although mesoporous films have many advantages such as excellent protective performance and high surface tension with water contact angle close to 90°, further improvement included that electrical conductivity is needed for them to meet the transportation applications.

Hence, in this paper, in order to improve the electrical conductivity of mesoporous C-SiO_2 film on substrates of 304 stainless steels, conductive polyaniline films were synthesized on mesoporous C-SiO_2 film by potentiostatic method. Then, the C-SiO_2-polyaniline films were pyrolyzed at low temperatures under N_2 atmosphere to obtain nitrogen-containing C-SiO_2 films. Electropolymerization process of aniline in sulfuric acid solution and some influential factors were investigated by potentiostatic method. Mesoporous carbon-silica-N film is used for the first time in this study as corrosion protective coating on 304 stainless steels. Characterization of the morphology of these mesoporous carbon-silica-N films and protective properties against corrosion exposed to sulfuric acid solution to simulate PEMFCs environment were also elucidated. The protective properties of the mesoporous carbon-silica-N coated 304 stainless steel against corrosion exposed to sulfuric acid solution were investigated to determine its potential application as an electrically conducting and corrosion-resistant coating for the metallic plates of PEMFCs.

2. Experimental

2.1. Chemicals

Triblock copolymer Pluronic F127 (M_w = 12,600, $PEO_{106}PPO_{70}PEO_{106}$) was purchased from Sigma–Aldrich Corp. Phenol, formalin solution, aniline, tetraethyl orthosilicate (TEOS), NaOH, HCl, H_2SO_4 and ethanol were purchased from Shanghai Chemical Corp. All chemicals were used as received without any further purification. Millipore water was used in all experiments.

2.2. Preparation and characterization of film

The low-molecular-weight resol (phenol–formaldehyde, M_w < 500) as a carbon source was prepared according to the procedure reported by the Zhao group [19]. Ordered mesoporous C-SiO_2 film was prepared according to the procedure reported by He et al. [12]. In a typical synthesis, 1.0 g of triblock copolymer Pluronic F127 was poured into 10.0 g of ethanol with vigorous stirring to obtain a clear solution. To this solution, 2.08 g of TEOS and 2.5 g of carbon source (20 wt% in ethanol) were added in succession. After stirring for 2 h, a homogeneous solution was obtained. The film was fabricated by spin-coating the solution onto clean type 304 stainless steel at 1500 rpm for 60 s. The film was aged at room temperature for 12 h and then thermopolymerized in an oven at 100 °C for 24 h. Then the resultant brown deposit was carbonized at 500 °C under N_2 atmosphere using always a heating rate of 1 °C min^{-1}, ordered mesoporous C-SiO_2 film was obtained.

Mesoporous PANI-C-SiO_2 film was prepared by the electropolymerization of aniline on mesoporous C-SiO_2 film with potentiostatic method. The electrolyte used for electropolymerization contained 0.2 M aniline and 0.5 M H_2SO_4 in an aqueous solution. The counter electrode was a platinum rod and a saturated calomel electrode (SCE) electrode was used as the reference electrode. The polyaniline-C-SiO_2 film was then pyrolyzed in a tubular furnace under N_2 atmosphere at 300 or 500 °C for 2 h using always a heating rate of 1 °C min^{-1}. Mesoporous nitrogen-containing C-SiO_2 films were obtained and denoted as C-SiO_2-N-*x*, where *x* represented the pyrolyzing temperature.

The field emission scanning electron microscopy (FE-SEM) images were obtained using Hitachi S-4800 microscope with an acceleration voltage of 30 kV, without any surface coating of the film samples. The films were determined by FTIR spectrophotometer using a Nicolet NEXUS-670 and KBr pellets of solid samples. Water contact angles were measured on a contact angle system SL200B (SOLON. Tech., China). The in-plane electrical conductivity was measured on the Wentworth Laboratories 6514 System Electrometer Keithley.

2.3. Electrochemical measurements

Thin film electrode leaving a circular area of 1 cm^{-2} used as working electrode in the electrochemical measurements. A saturated calomel electrode and a platinum foil were used as the reference electrode and the counter electrode, respectively. All electrochemical experiments were carried out in 0.5 mol L^{-1} H_2SO_4 aqueous solution. The film electrodes were stabilized in the solution at open circuit for 60 min. An electrochemical interface (Solartron 1287) and a conventional three-electrode system were employed to conduct potentiodynamic polarization measurements at a scan rate of 10 mV s^{-1}. Potentiostatic polarizations were conducted on a Solartron 1287, to investigate the performance and stability of the films, the polarizations were

Table 1
The corrosion current density (i_{corr}) and the corrosion potentials (E_{corr}) values for the mesoporous composite films in 0.5 M H_2SO_4.

Sample	Electropolymerization potential (V) (SCE)	Electropolymerization time (s)	E_{corr} (mV) (SCE)	i_{corr} ($\mu A\,cm^{-2}$)
C-SiO_2	0	0	187	0.75
PANI-C-SiO_2	0.85	200	51	1.2
PANI-C-SiO_2	0.85	250	78	0.46
PANI-C-SiO_2	0.85	300	85	2.5
PANI-C-SiO_2	0.85	400	42	4.9
PANI-C-SiO_2	0.90	250	292	0.13
PANI-C-SiO_2	0.95	250	−251	3.9

recorded at applied anode potential of −100 mV (SCE) and cathode potential +600 mV (SCE) for PEMFCs. Potentiostatic polarizations were conducted at room temperature and 80 °C. Electrochemical impedance spectroscopy (EIS) measurements using Solartron 1260 frequency response analyser coupled to Solartron 1287 potentiostat were obtained at frequencies between 100 kHz and 0.01 Hz. The amplitude of the sinusoidal potential signal was 10 mV.

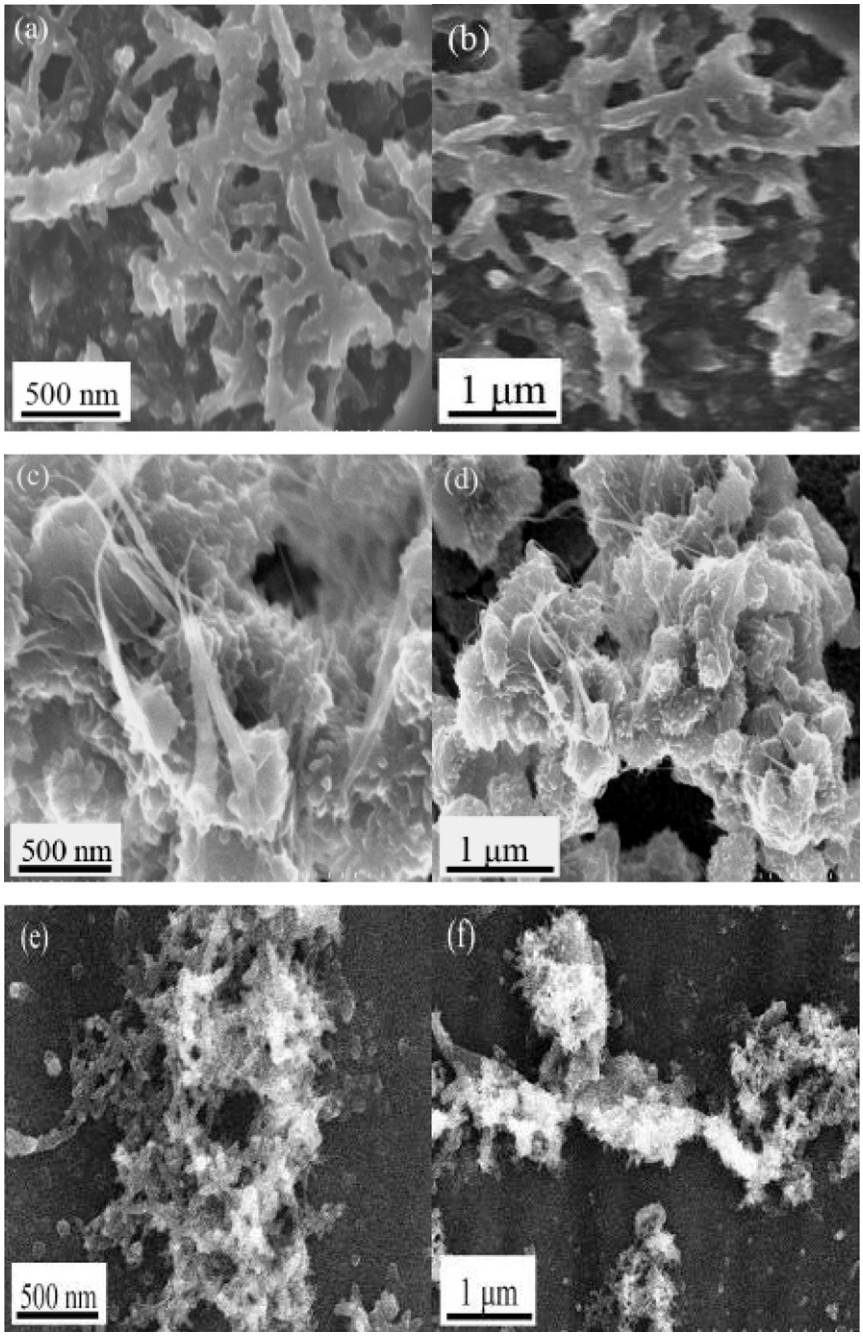

Fig. 4. SEM images of the PANI-C-SiO_2 films synthesized by varying the potentiostatic conditions: 0.85, 0.90 and 0.95 V (SCE) with an electropolymerization time of 250 s in 0.5 mol L^{-1} H_2SO_4 solution.

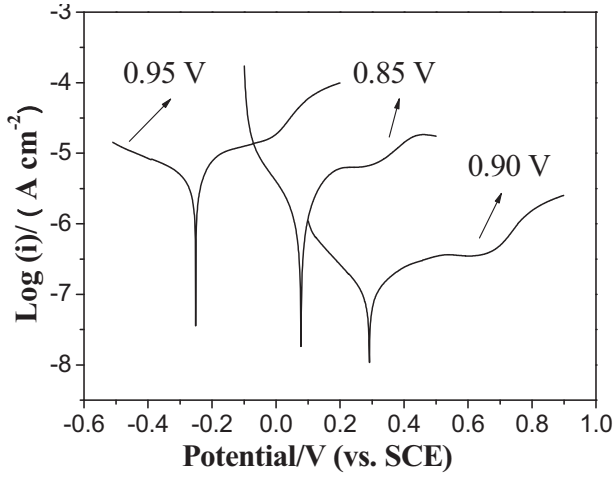

Fig. 5. Potentiodynamic polarization curves of the PANI-C-SiO_2 films synthesized by varying the potentiostatic conditions: 0.85, 0.90 and 0.95 V (SCE) with an electropolymerization time of 250 s in 0.5 mol L^{-1} H_2SO_4 solution.

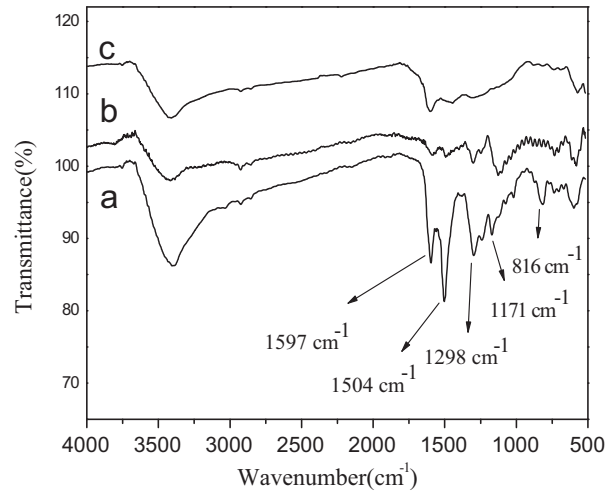

Fig. 6. FT-IR spectrum of (a) PANI-C-SiO_2, (b) C-SiO_2-N-300, and (c) C-SiO_2-N-500.

3. Results and discussion

3.1. Potentiostatic polymerization of aniline on mesoporous C-SiO_2 film – effect of the electropolymerization time

The electrochemical polymerization of the aniline on mesoporous C-SiO_2 film was carried out in 0.5 M H_2SO_4 containing 0.2 M aniline by potentiostatic method. To investigate the effect of the electropolymerization time on the structure and corrosion properties of the resulting films, the samples were characterized by current–time transient, SEM and potentiodynamic polarization measurements. Fig. 1 illustrates the simulative and actual current–time curves traced during the potentiostatic polymerization of aniline at different applied potentials. It is shown that the actual current–time curves in all cases are in agreement with the simulative current–time curves. We can see that the current decreases (region ab in Fig. 1(a)) within very short times in all cases due to the passivation of 304SS. The initial current drop in these cases is followed by a steady-state limiting value (region bc in Fig. 1(a)), which is attributed to the start of transpassivity at higher potentials [20]. In the presence of aniline, two main regions I and II in Fig. 1 can be distinguished in each curve after the initial drop of the current due to the 304SS passivation [21]. The first region I is characterized by an increase of the current due to the aniline oxidation along with a nucleation process, leading to the formation of the PANI film. As shown in Fig. 1(b), the time needed for the nucleation process decreases as the applied potential becomes more positive. The second region II starts by the decrease of the current at 0.90 and 0.95 V (SCE) (similar to the region de in Fig. 1(a)), while the second region II starts by the trend of the current to attain a steady-state value as is shown at 0.85 V. It seems that the current–time behavior at longer times of the polymer growth, within the region II, depends on the applied potential and thereby on the oxidation state and amount of PANI. Increasing the constant potential during the potentiostatic polymerization of aniline results in the increase of the polymerization rate, a measure of which might be the moment at which the current attains its sharp value. For instance, Fig. 1(b) shows that this moment is at ~90 and 200 s for the constant potential of 0.95 and 0.85 V (SCE), respectively. The decrease in the current in region II (Fig. 1(b), similar to the region de in Fig. 1(a)) indicates the predominance of the degradation over the polymerization whereas the increase in current at longer times suggests an opposite behavior [22]. An almost steady state current observed at the constant potential of 0.85 V (SCE) in Fig. 1(b) (similar to the region de in Fig. 1(a)) suggests that polymerization and degradation occur at approximately equal rates.

Table 2
The electrical conductivity, the corrosion current density (i_{corr}) and the corrosion potentials (E_{corr}) values for the mesoporous composite films in 0.5 M H_2SO_4.

Sample	i_{corr} ($\mu A\,cm^{-2}$)	E_{corr} (mV) (SCE)	G ($S\,m^{-1}$)
C-SiO_2	0.75	187	0.00168
PANI-C-SiO_2	0.46	78	38.62
C-SiO_2-N-300	2.97	110	3.61
C-SiO_2-N-500	0.59	−8	1.24

Fig. 2 shows SEM images of the C-SiO_2 film and the PANI/C-SiO_2 films synthesized by 200–400 s. It can be observed that an interconnected porous fibrillar-like morphology was obtained in the cases of aniline and H_2SO_4 media. Such similar fibrillar morphology has been previously obtained for polyanilines prepared using several other conditions [23–25]. At the initial stage (Fig. 2(a) and (b)), this fibrillar-like morphology was obtained for those polymers that exhibited a progressive nucleation. As the loading of deposited PANI increases (Fig. 2(c) and (d)), the diameter of the

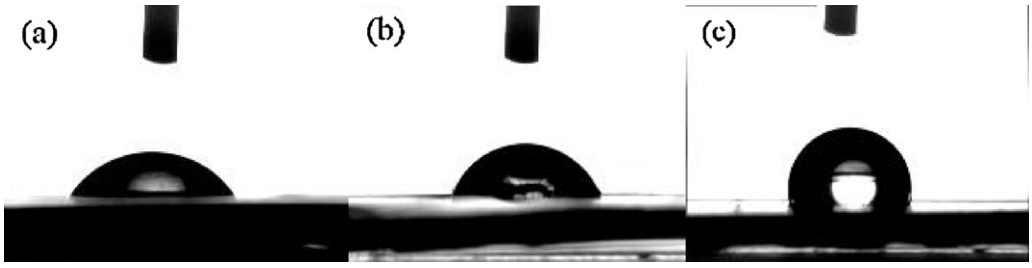

Fig. 7. The contact angles of (a) PANI-C-SiO_2, (b) C-SiO_2-N-300, and (c) C-SiO_2-N-500.

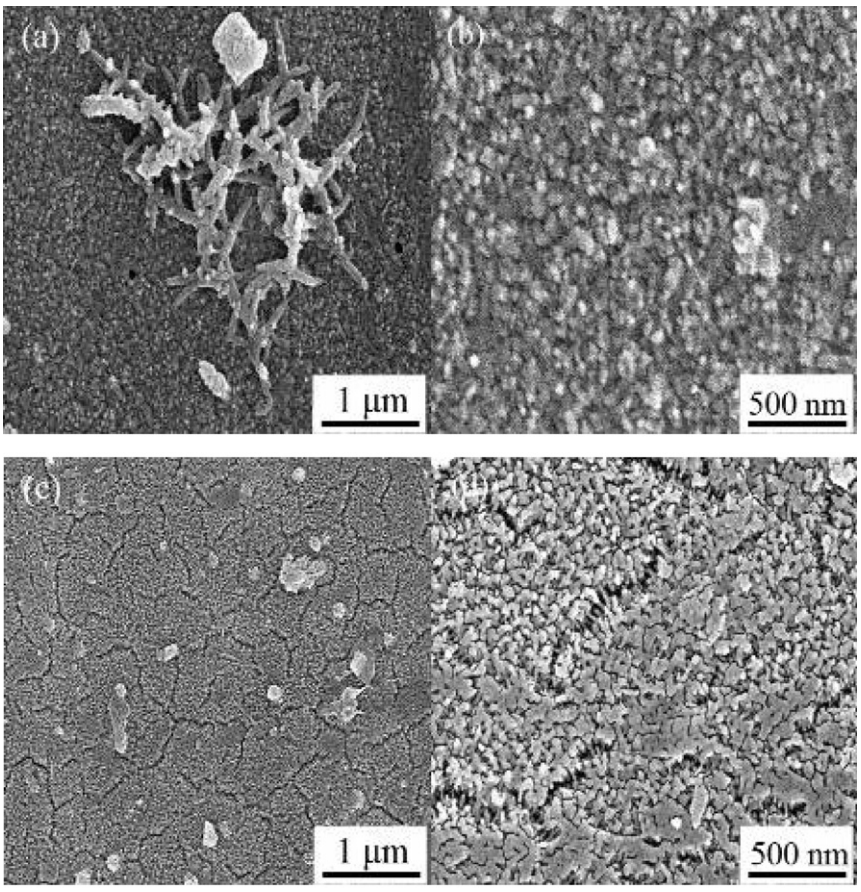

Fig. 8. SEM images of (a and b) C-SiO_2-N-300 and (c and d) C-SiO_2-N-500.

PANI increases continuously and then the fibrillar-like PANI begins growing breadthwise. As the electropolymerization time reaches 300 s (Fig. 2(e) and (f)), the morphology is much more compact with a globular-like aspect. Beyond the electropolymerization time of 400 s (Fig. 2(g)), the PANI is deposited compactly around the surface of the C-SiO_2 film, but the crack phenomenon has occurred on some areas. These results indicate that the electropolymerization time of PANI should not exceed 300 s and these phenomena have profoundly implicated on the corrosion behavior of the PANI-C-SiO_2 films.

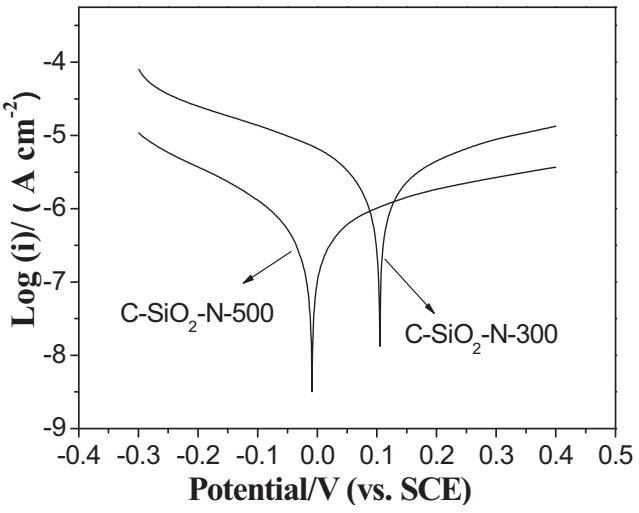

Fig. 9. Potentiodynamic polarization curves of C-SiO_2-N-300 and C-SiO_2-N-500 in 0.5 mol L^{-1} H_2SO_4 solution.

Fig. 3 shows the potentiodynamic polarization curves for C-SiO_2 coated 304SS and for PANI-C-SiO_2 coated 304SS after immersion in 0.5 M H_2SO_4 for 1 h. The corrosion potential and corrosion current determined by potentiodynamic polarization extrapolations for these films are shown in Table 1. PANI-C-SiO_2 films are found to be effective in reducing the corrosion rate of 304SS, while the free corrosion potential and the free corrosion current density of the bare 304SS in sulfuric acid are about −180 mV (SCE) and 8.9 μA cm^{-2}, respectively [12]. As the electropolymerization time increases, the crack phenomenon of the PANI occurred on some areas and then a nonuniform PANI coating is obtained, which is discussed in SEM images. However, a nonuniform PANI coating has been found to accelerate general corrosion of metal substrate in a free corrosion condition [26]. These results suggest that the optimal time of electropolymerization is 250 s to be most effective in reducing the corrosion rate, when the applied potential of electropolymerization is 0.09 V (SCE).

Table 3
Fitted results of electrochemical impedance spectra.

Sample	R_s (Ω cm^2)	CPE (μF cm^{-2})	R_{ct} (Ω cm^2)	$W_0 - T$
MCF/PANI	2.589	20	88.01	2.492
MCF/PANI-300	6.768	46	2543	1.992
MCF/PANI-500	8.468	759	2834	0.563

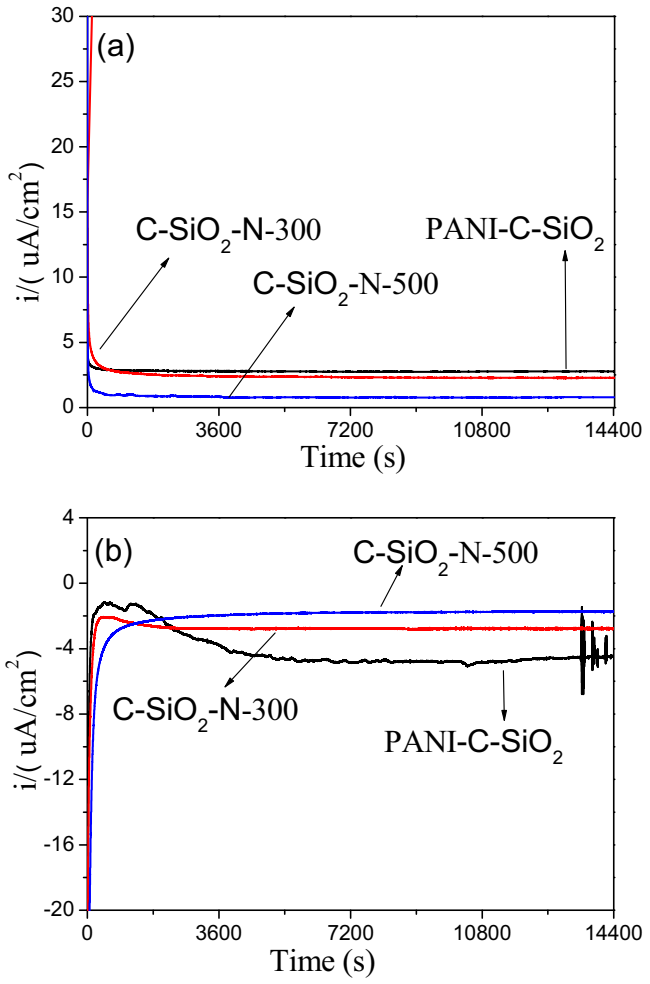

Fig. 10. Potentiostatic polarization curve of PANI-C-SiO_2, C-SiO_2-N-300, and C-SiO_2-N-500 at 600 mV (SCE) (a) and −100 mV (SCE) (b) in 0.5 mol L^{-1} H_2SO_4 solution.

3.2. Potentiostatic polymerization of aniline on mesoporous C-SiO_2 film – effect of the applied potential

To investigate the influence of the applied potential on aniline polymerization, electropolymerization was conducted by 250 s with different applied potentials of 0.85, 0.90, and 0.95 V. From Fig. 1(b), we know that increasing the applied potential during the potentiostatic polymerization of aniline results in two opposite effects [21]. Fig. 4 illustrates the SEM images of the PANI-C-SiO_2 films during the potentiostatic polymerization of aniline at different applied potentials (E_{appl}) in 0.5 M H_2SO_4 solution. As shown in Fig. 4, PANI exhibits nanofibrous structures in the 0.85 V (SCE), while PANI exists in flower shapes in the 0.90 V (SCE). When the applied potential increases, two-dimensional growth of PANI is promoted, resulting in better array. However, the PANI film obtained through conventional potentiostatic deposition at 0.95 V has a brush-fire coil-like and loose conformation (Fig. 4(e) and (f)). The polymerization around the embryonic nuclei should be faster at higher potentials because the transient concentration of PANI molecules is much higher. These films display different surface morphologies, indicating that the potential used for aniline polymerization is a key factor for the obtained conformation in the PANI film [27]. Therefore, the PANI film prepared at 0.90 V (SCE) shows a sufficient homogeneous form indicating the polymer acts as a physical barrier to corrosion.

Fig. 5 shows the potentiodynamic curves of the PANI-C-SiO_2 films synthesized by different applied potentials in 0.5 M H_2SO_4. The values of the corrosion potential (E_{corr}) and corrosion current density (i_{corr}) obtained from these curves are also given in Table 1. Analysis of these data shows that i_{corr} decreases significantly when PANI is electrodeposited at 0.85 V or 0.90 V (SCE). From the discussion of Fig. 4, we find that the PANI-C-SiO_2 film synthesized at 0.95 V has a brush-fire coil-like and loose conformation, which could be desquamated during operation, resulting in a big corrosion current density.

3.3. Effect of calcination temperatures of PANI-C-SiO_2 films on their protective ability against corrosion of 304SS

The structural characteristics of samples were investigated by FT-IR spectroscopy in the range 4000–500 cm^{-1}, as shown in Fig. 6. These peaks of PANI-C-SiO_2 are in accordance with the characteristic peaks of PANI reported in the literatures [28]. It is found that the polyaniline film formed by potentiostatic method has both benzenoid and quinoid moieties. The peak at about 1597 cm^{-1} is duo to the C=C double bond of the quinoid rings, whereas the peak at 1504 cm^{-1} arises due to vibration of the C=C bond associated with the benzenoid ring [29–31]. Aromatic C–N stretching is responsible for the clustering of peaks between 1320 cm^{-1} and 1120 cm^{-1} [29,32]. The peak at 816 cm^{-1} is due to the bending of the aromatic C–H bond [32]. The PANI-C-SiO_2 film was then pyrolyzed under N_2 atmosphere at 300 or 500 °C to obtain C-SiO_2-N-300 and C-SiO_2-N-500, respectively. Most of the typical peaks of PANI in Fig. 6(c) disappear and only those of C=C and C–N are detected. It indicates the almost complete removal of PANI and the formation of a nitrogen-containing C-SiO_2 film.

Surface energy of bipolar plates is other important factor affecting cell performance particularly at high current densities since water produced by the cathode reaction should be immediately removed to avoid flooding and power degradation due to catalyst submergence [33]. Therefore, bipolar plates with low surface energy, low water contact angle (>90° and high) surface wetability could directly contribute to flooding of cathode side of the fuel cell. The contact angles of the samples with water are shown in Fig. 7. In general, PANI is hydrophilic, and after pyrolyzed at 300 °C, it still maintains some hydrophilic groups (Fig. 6(b)). When the PANI-C-SiO_2 was pyrolyzed at 500 °C, its carbonization began, and those hydrophilic groups were lost (Fig. 6(c)). According to the test data, the PANI-C-SiO_2 and the C-SiO_2-N-300 are hydrophilic, while the C-SiO_2-N-500 with a water contact angle 95° would be helpful for water removal in the stack and beneficial to the simplification of water management.

As shown in Fig. 8, the pyrolyzed temperature has a great influence on the morphology of the PANI-C-SiO_2 films. Fig. 8(a) and (b) shows that a few nanofibre structures indicating that PANI has been pyrolyzed partially at 300 °C. As the pyrolyzed temperature increases to 500 °C, there is not almost PANI in Fig. 8(c) and (d). As shown in Fig. S3, the C-SiO_2-N-500 film is pin-hole free in the contacting layer. Fig. 9 presents the potentiodynamic polarization curves for the mesoporous C-SiO_2-N films in 0.5 mol L^{-1} H_2SO_4 aqueous solution at room temperature. The electrical conductivity, corrosion potential and corrosion current determined by potentiodynamic polarization extrapolations for these films are shown in Table 2. It shows that the mesoporous C-SiO_2-N-500 film has a low corrosion current, a perfect water contact angle and an electrical conductivity, signifying the good protective performance.

Fig. 10(a) shows the potentiostatic polarization curve of the composite films coated 304 stainless steel in 0.5 mol L^{-1} H_2SO_4 solution at +600 mV (SCE). The polarization current of PANI-C-SiO_2 decreased slowly with time to the level of 2.7 μA cm^{-2}. However, the polarization current of C-SiO_2-N-500 film decreased instantly with time to the level of 0.8 μA cm^{-2}, significantly lower than the passive current for the PANI-C-SiO_2 film. Besides, the C-SiO_2-N-300

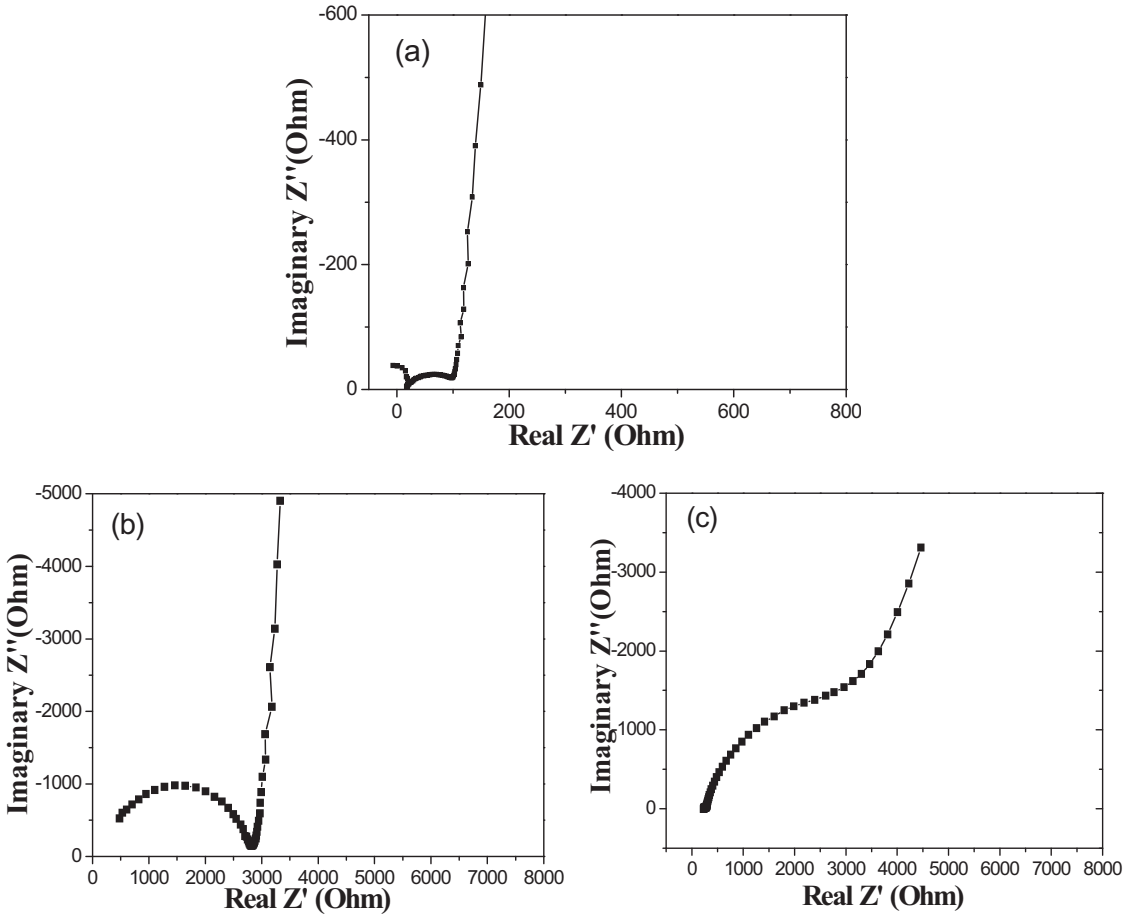

Fig. 11. Electrochemical impedance spectra of PANI-C-SiO_2 (a), C-SiO_2-N-300 (b), and C-SiO_2-N-500 (c) in 0.5 M H_2SO_4.

and C-SiO_2-N-500 films are quite stable during the polarization, as is evidenced by the absence of the current density fluctuation, suggesting no degradation is observed after potentiostatic measurements and indicating the composite films are very stable at the cathode working potential of PEMFC. It is clear that the C-SiO_2-N-500 film inhibits effectively the corrosion of the substrate steel. Fig. 10(b) shows the potentiostatic polarization curve of the composite films coated 304 stainless steel in 0.5 mol L^{-1} H_2SO_4 solution at −100 mV (SCE). The polarization current density of C-SiO_2-N-500 film decreased significantly to a steady value of around −1.8 μA cm^{-2}. No degradation was observed after potentiostatic measurements for 4 h, indicating the high stability of C-SiO_2-N-500 film at the anode working potential of PEMFC.

The results obtained in both anodic and cathodic conditions imply that coated with C-SiO_2-N-500 film, the 304 stainless steel has lower polarization current than the data of previous reports in simulated PEMFCs environments at room temperature [34,35]. The range of normal working temperature of PEMFCs is 60–80 °C, so most of the research works investigate the stability of the bipolar plates at 70 or 80 °C. In this paper, we also investigate the stability of the films at applied anode potential of −100 mV (SCE) and cathode potential +600 mV (SCE) at 80 °C. As shown in Figs. S1 and S2, the C-SiO_2-N-500 film has less and steady polarization current density than PANI-C-SiO_2 film. Because of the high working temperature, all potentiostatic polarization curves are not smoothness like most of reports [8,36–39]. The polarization current density of the C-SiO_2-N-500 film stabilizes in the range of 1.4–2.4 μA cm^{-2} in simulated cathode condition, and maintains at −2 μA cm^{-2} in simulated anodic condition, which are lower than recent reports on the bipolar plates [6,37,39–45].

3.4. Electrochemical impedance measurements

The electrochemical impedance spectra for the PANI-C-SiO_2 and C-SiO_2-N coatings deposited on 3304SS in 0.5 mol L^{-1} H_2SO_4 are shown in Fig. 11. The corresponding equivalent circuits are proposed to fit the impedance plots as seen in Fig. 12. An interesting feature of the impedance plot can be observed in Fig. 11(a). The negative Faradaic impedance of the PANI-C-SiO_2 can be observed that are drastically different from the C-SiO_2-N. Such a phenomenon from positive to negative Faradaic impedance suggests the presence of an inductive component (L) in the PANI-C-SiO_2 film [46,47]. R_s is the solution resistance and R_{ct} is the charge-transfer resistance. The constant phase element (CPE) is accounted for the adsorptive

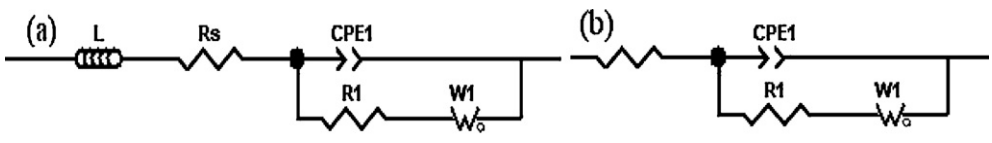

Fig. 12. Equivalent circuits representing the corrosion of the PANI-C-SiO_2 (a) and the C-SiO_2-N (b) in 0.5 mol L^{-1} H_2SO_4 solution.

double-layer capacitance of non-homogeneity interface. W_0 is the diffusion impedance and $W_0 - T$ is the Warburg coefficient. The fitting parameters using Zview-impedance analysis software 2.80 present in Table 3.

Comparing the EIS data of the PANI-C-SiO_2 and C-SiO_2-N coated 304SS, we can see that the electrochemical impedance values of the C-SiO_2-N coated samples are significantly higher than the PANI-C-SiO_2 sample, and the negative Faradaic impedance disappeared suggests that PANI has been pyrolyzed. Wherein, C-SiO_2-N-500 film shows a larger semi-arc-shaped radius and a lower $W_0 - T$ coefficient, indicating that its impedance in the electrochemical corrosion process is big, the corrosion products are slow in the diffusion process of the film. Therefore, C-SiO_2-N-500 film exhibits high stability in H_2SO_4 solution, and is effective barrier to the inward penetration of test solution, and thus reduces significantly the corrosion of the substrate alloy.

4. Conclusions

We demonstrate the formation of mesoporous carbon-silica-polyaniline on 304SS substrate and provide a simple route to obtain nitrogen-containing carbon-silica films. Comparing the polyaniline coatings formed using the different electropolymerization time and applied potential, the morphologies are quite different. The potentiodynamic tests show that the best potentiostatic condition is electropolymerization 250 s at the applied potential of 0.09 V (SCE), corresponding corrosion potential and corrosion current density are 292 mV and 0.13 $\mu A\,cm^{-2}$, respectively. Wherein, the nitrogen-containing carbon-silica film shows the optimal protective performance and a high stability compared with mesoporous carbon-silica-polyaniline. The enhancement of the performance is attributed to the high surface tension with water contact angle close to 90°. We believe that the mesoporous C-SiO_2-N films have a potential application as a protect coating of bipolar plate material.

Acknowledgment

The authors appreciate the financial supports of the National Natural Science Foundation of China (50871053).

Appendix A. Supplementary data

Supplementary data associated with this article can be found, in the online version, at doi:10.1016/j.jpowsour.2011.07.084.

References

[1] V. Mehta, J.S. Cooper, J. Power Sources 1 (2003) 32–53.
[2] A. Schäfer, J.B. Heywood, M.A. Weiss, Energy 31 (2006) 2064–2087.
[3] R.F. Silva, D. Franchi, A. Leone, L. Pilloni, A. Masci, A. Pozio, Electrochim. Acta 51 (2006) 3592–3598.
[4] D.P. Davies, P.L. Adcock, M. Turpin, S.J. Rowen, J. Appl. Electrochem. 30 (2000) 101–105.
[5] H. Tawfik, Y. Hung, D. Mahajan, J. Power Sources 163 (2007) 755–767.
[6] Y. Wang, D.O. Northwood, J. Power Sources 165 (2007) 293–298.
[7] Y.J. Ren, J. Chen, C.L. Zeng, J. Power Sources 195 (2010) 1914–1919.
[8] Y.B. Lee, C.H. Lee, D.S. Lim, Int. J. Hydrogen Energy 34 (2009) 9781–9787.
[9] C.Y. Chung, S.K. Chen, P.J. Chiu, M.H. Chang, T.T. Hung, T.H. Ko, J. Power Sources 176 (2008) 276–281.
[10] T. Fukutsuka, T. Yamaguchi, S.I. Miyano, Y. Matsuo, Y. Sugie, Z. Ogumi, J. Power Sources 174 (2007) 199–205.
[11] A. Hermann, T. Chaudhuri, P. Spagnol, Int. J. Hydrogen Energy 30 (2005) 1297–1302.
[12] T. Wang, J.P. He, D. Sun, J.H. Zhou, Y.X. Guo, X.C. Ding, S.C. Wu, J.Q. Zhao, J. Tang, Corros. Sci. 53 (2011) 1498–1504.
[13] S. Kitta, H. Uchida, M. Watanabe, Electrochim. Acta 4 (2007) 2025–2033.
[14] C.Y. Chung, S.K. Chen, T.S. Chin, T.H. Ko, S.W. Lin, W.M. Chang, S.N. Hsiao, J. Power Sources 186 (2009) 393–398.
[15] G. Bereket, E. Hür, Y. Şahin, Appl. Surf. Sci. 252 (2005) 1233–1244.
[16] A. Yağan, N.Ö. Pekmez, A. Yıldız, Electrochim. Acta 51 (2006) 2949–2955.
[17] S. Joseph, J.C. McClure, R. Chianelli, P. Pich, P.J. Sebastian, Int. J. Hydrogen Energy 30 (2005) 1339–1344.
[18] M.B. González, S.B. Saidman, Corros. Sci. 53 (2011) 276–282.
[19] Y. Meng, D. Gu, F.Q. Zhang, Y.F. Shi, H.F. Yang, Z. Li, C.Z. Yu, B. Tu, D.Y. Zhao, Angew. Chem. Int. Ed. 44 (2005) 7053–7059.
[20] W. Lou, K. Ogura, Electrochim. Acta 40 (1995) 667–672.
[21] D. Sazou, M. Kourouzidou, E. Pavlidou, Electrochim. Acta 52 (2007) 4385–4397.
[22] K. Aoki, S. Tano, Electrochim. Acta 50 (2005) 1491–1496.
[23] H. Zhang, G.P. Cao, W.K. Wang, K.G. Yuan, B. Xu, W.F. Zhang, J. Cheng, Y.S. Yang, Electrochim. Acta 54 (2009) 1153–1159.
[24] A.J. Motheo, J.R. Santos, E.C. Venancio, L.H.C. Mattoso, Polymer 39 (1998) 6977–6982.
[25] C.Q. Cui, L.H. Ong, T.C. Tan, J.Y. Lee, Synth. Met. 58 (1993) 147–160.
[26] T. Wang, Y.J. Tan, Mater. Sci. Eng. B 132 (2006) 48–53.
[27] H.F. Jiang, X.X. Liu, Electrochim. Acta 55 (2010) 7175–7181.
[28] C.T. Kuo, S.A. Chen, G.W. Hwang, H.H. Kuo, Synth. Met. 93 (1998) 155–160.
[29] J. Tang, X. Jing, B. Wang, E. Wang, Synth. Met. 24 (1988) 231–238.
[30] K.G. Neoh, E.T. Kang, K.L. Tan, J. Phys. Chem. 95 (1991) 10151–10156.
[31] T. Ohsaka, Y. Ohnuki, N. Oyama, G. Katagiri, K. Kamisako, J. Electroanal. Chem. 161 (1984) 399–406.
[32] S. Quillard, G. Louran, S. Lefrant, A.G. MacDiarmid, Phys. Rev. B 50 (1994) 12496–12508.
[33] E.A. Cho, U.S. Jeon, S.A. Hong, I.H. Oh, S.G. Kang, J. Power Sources 1-2 (2005) 177–183.
[34] S.K. Chen, H.C. Lin, C.Y. Chung, Corrosion resistance study of stainless steel bipolar plates with NiAl coatings, Feng Chia University and National Science Council of Republic of China Under the Grant Numbers FCU-93GB27 and NSC 93-2218-E-35-006.
[35] Y.J. Ren, C.L. Zeng, J. Power Sources 2 (2007) 778–782.
[36] M. Zhang, B. Wu, G.Q. Lin, Z.G. Shao, M. Hou, B.L. Yi, J. Power Sources 196 (2011) 3249–3254.
[37] A.G. Howell, H.L. Wang, S.W. Cowley, J.A. Turner, J. Power Sources 196 (2011) 5922–5927.
[38] R.J. Tian, J. Power Sources 196 (2011) 1258–1263.
[39] Y. Wang, D.O. Northwood, J. Power Sources 163 (2006) 500–508.
[40] M. Xiao, Y. Lu, S.J. Wang, Y.F. Zhao, Y.Z. Meng, J. Power Sources 160 (2006) 165–174.
[41] K.H. Cho, W.G. Lee, S.B. Lee, H. Jang, J. Power Sources 2 (2008) 671–676.
[42] V.V. Nikam, R.G. Reddy, S.R. Collins, P.C. Williams, G.H. Schiroky, G.W. Henrich, Electrochim. Acta 6 (2008) 2743–2750.
[43] K.H. Lee, S.H. Lee, J.H. Kim, Y.Y. Lee, Y.H. Kim, M.C. Kim, D.M. Wee, Int. J. Hydrogen Energy 3 (2009) 1515–1521.
[44] Y. Wang, D.O. Northwood, J. Power Sources 1 (2008) 40–48.
[45] H. Wang, J.A. Turner, J. Power Sources 2 (2007) 387–394.
[46] W. Chen, J.M. Kim, S.H. Sun, S. Chen, Phys. Chem. Chem. Phys. 23 (2006) 2779–2786.
[47] G. Markovich, C.P. Collier, J.R. Heath, Phys. Rev. Lett. 80 (1998) 3807–3810.